

PVP2015-45811

WEAR INDUCED BY STOCHASTIC SLIDING IMPACTS

Thibaut Souillart

Laboratoire de Tribologie et Dynamique des Systèmes, UMR CNRS 5513,
 Ecole Centrale de Lyon, Université de Lyon,
 36, avenue Guy de Collongue, F-69134 Ecully, France
 Commissariat à l'Energie Atomique et aux Energies Alternatives CEA-Saclay,
 DEN, DM2S, SEMT, DYN, F-91191 Gif-sur-Yvette, France.

Emmanuel Rigaud

Laboratoire de Tribologie et
 Dynamique des Systèmes, UMR
 CNRS 5513, Ecole Centrale de
 Lyon, Université de Lyon, 36,
 avenue Guy de Collongue, F-
 69134 Ecully, France

Alain Le Bot

Laboratoire de Tribologie et
 Dynamique des Systèmes, UMR
 CNRS 5513, Ecole Centrale de
 Lyon, Université de Lyon, 36,
 avenue Guy de Collongue, F-
 69134 Ecully, France

Christian Phalippou

Commissariat à l'Energie
 Atomique et aux Energies
 Alternatives CEA-Saclay, DEN,
 DM2S, SEMT, DYN,
 F-91191 Gif-sur-Yvette, France.

ABSTRACT

Vibrations of the steam generator tubes in nuclear power plants induce stochastic impacts between the tubes and the supports. As a consequence, wear is generated. A test rig is designed and used to perform impacts between two metal cylinders with various incidence angles and impact velocities. The normal and tangential components of the contact load are measured during the tests. Rate and duration of impacts, instantaneous ratio between normal and tangential loads for each impact are deduced. Influence of incidence angle and impact velocity on impact duration, ratio between tangential load and normal load during impact and wear volume is highlighted.

NOMENCLATURE

e	Restitution coefficient of impact
f	Excitation frequency
f_0	First natural frequency of impactor
k	Stiffness of impactor
m	Impacting mass
t	Time
$t_{imp} ; \overline{t_{imp}}$	Duration of impact
E^*	Equivalent Young's modulus
$F_n ; \overline{F}_n$	Maximum of the normal component of load measured during impact

$F_t ; \overline{F}_t$	Maximum of the tangential component of load measured during impact
R^*	Equivalent radius
T^*	Normalized shear energy
V	Impacting velocity
W_{imp}	Wear volume per impact
W_{tot}	Wear volume for an entire test
$\alpha ; \overline{\alpha}$	Incidence angle of impactor
$\mu ; \overline{\mu}$	Instantaneous ratio between normal and tangential loads during impact
δ_n	Depth of indentation (approach)
δ_t	Sliding distance
λ	Particle shape coefficient
μ_c	Critical friction coefficient
\overline{X}	Average value of X for an entire test

INTRODUCTION

Heat exchangers of Pressurized Water Reactor (PWR) are composed of thousands of tubes supported by baffles and Anti-Vibration Bars (AVB). Functional clearances are needed between tubes and bars because of thermal expansion and assembly purposes. In steam generators, tubes are excited by high flow rates. This excitation could lead to a dynamic response

characterized by sliding impacts between tubes and AVB and generate wear [1].

Several types of wear exist according to the motions and the bodies involved [2]. Sliding impacting is usually studied as an erosive and percussive process which leads to both surface and volume degradation. Surface degradation can be associated with adhesion [3] (metal transfer due to sheared asperities junctions) and abrasion [4] (cutting of the rubbing surface by hard asperities). Volume degradation is often described as the formation and propagation of subsurface fatigue cracks in the material (delamination).

Engel [5–7] develops a model to predict impact wear based on surfaces conformance in terms of wear formation and a strong dependence with shear stress concerning wear evolution during time. Levy [8] proposes a model based on a proportionality with load and sliding distance during impact. Connors [9], Frick [10] and Hoffman [11] also propose impact wear models derived from Archard equation. The wear law proposed by Lewis includes both a term derived from Engel model and a dependency with sliding distance [12].

Erosion results from the impact of streams of solid particles on a surface and not from the impact of two macroscopic bodies. Nevertheless, asperities which constitute the contact have a size similar to erosive particles and kinetic energy of the solid impactor and an erosive particle have the same order of magnitude. Therefore, erosive models can be relevant to describe wear of macroscopic bodies [13,14].

An experimental work is performed in order to confirm this hypothesis and to highlight influence of test parameters on wear volume. First section presents the test rig that have been designed and used to generate impacts with various incidence angles and velocities. Load and wear measurement protocols, wear conditions and testing parameters are explained. Second section goes through the obtained impact characteristics in terms of load evolution during impact and generated wear. Experimental results are shown in the third section. Influence of incidence angle and impact velocity on impact duration, ratio between tangential and normal loads during impact and wear volume is highlighted and discussed.

PRINCIPLE OF EXPERIMENT

Test rig

The test rig is shown in Figure 1. Two shakers are placed at $\pm 45^\circ$ to the vertical and excite a hard steel cylinder sample. Two identical springs with the same stiffness ($k = 590 \text{ N/m}$) provide the connection between the shaker and the sample holder ($m = 0.17 \text{ kg}$). Thus, the natural frequency f_0 of the impactor is 9.5 Hz.

The incidence angle α to the horizontal is obtained by setting a specific ratio between the amplitudes of each of the two shakers sinusoidal inputs. Therefore, any test with an incidence angle between 10° and 90° can be performed.

During its motion, the impactor hits a mild steel cylinder sample that is expected to wear. Cylinders are crossed so that a point contact is obtained.

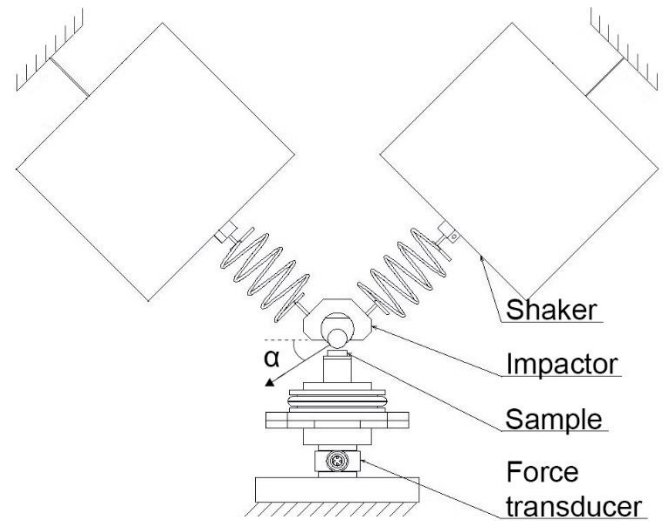


FIGURE 1. TEST RIG.

Test samples

The impactor cylinder ($\varnothing = 7 \text{ mm}$, $L = 7 \text{ mm}$) has a Vickers hardness of 820 Hv whereas the target ($\varnothing = 7 \text{ mm}$, $L = 7 \text{ mm}$) hardness is equal to 145 Hv. Both have a Young modulus of 200 GPa.

Load measurement protocol and signal processing

The three components of the contact load are measured by a 3-axis piezoelectric load transducer placed behind the sample. Its stiffness is equal to $740 \text{ N}/\mu\text{m}$ for the Z component and $170 \text{ N}/\mu\text{m}$ for the X and Y components. The mass supported by the load transducer is about 0.1 kg (sample and sample holder), so the measure of the contact load is accurate up to 7 kHz for the tangential components and 14 kHz for the normal component. Signals are acquired with a dynamic signal acquisition card and a high sampling rate of 50 kHz in order to correctly measure contact load during impact.

A complete acquisition of the contact load during the full length of the test is impossible due to storage space limitations. Therefore, signals are acquired during 1500 evenly distributed acquisition windows of 1 second.

Signals are processed in order to automatically find each impact and retrieve the impact rate, flight and contact times, normal and tangential components of the contact load during impact. Ratio between maxima of tangential and normal loads μ is then calculated for each impact.

Wear conditions and testing parameters

All tests are performed with the following characteristics. The test duration is 17 h, the excitation frequency f is chosen about 30 Hz and the excitation levels of the shakers are adjusted in order to obtain a maximal normal load during impact of 12 N in average. The Hertz theory applied to an equivalent static contact predicts a maximal contact pressure about 1.5 GPa, a contact diameter of $120 \mu\text{m}$ and a depth of indentation δ_n of $2.1 \mu\text{m}$. As the actual contact area is smaller than the apparent one,

pressure would be concentrated at the top of surface asperities and could generate local plastic deformation.

Moderate contact loads are applied to focus more on erosive wear than on fatigue or delamination. The set of parameters is chosen to get a substantial amount of wear in a relative short time.

Wear volume analysis

At the end of a test, worn sample is removed from test rig and wear scars are analyzed with an optical interferometer (Figure 2). Negative, positive and natural volumes of wear are then retrieved.

Uncertainty on volume is calculated based on uncertainties of the interferometer measurement and the surface adjustment. Minimal wear volume that can be measured is estimated at 10^{-3} mm³.

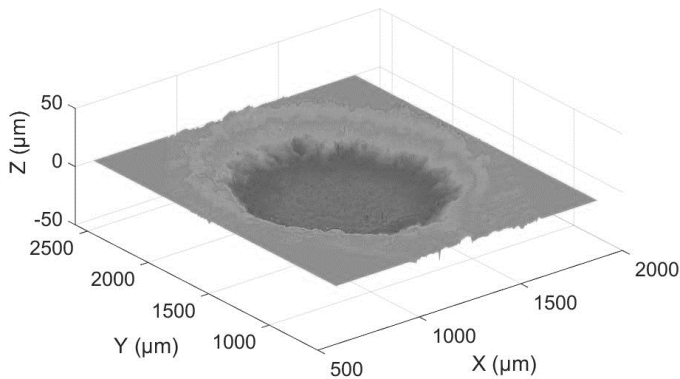


FIGURE 2. INTERFEROGRAM OF A WEAR SCAR

IMPACTS CHARACTERISTICS

Large time scale

Figure 3 shows time evolution of normal load during 1 s. Impacts are clearly distinguishable as quick variations of contact load. A free flight period separate two successive main impacts which usually last about 50 ms. Some main impacts are followed by multiple lower amplitude impacts during a short period (about 30 ms). It can be understood as successive rebounds of the impactor that occur after the main impact. As a result, the impact rate differs from excitation frequency. During a 17 hours duration test, the total number of impacts typically ranges from 1.8 to 3.7 million that is to say from 30 to 60 impacts per second.

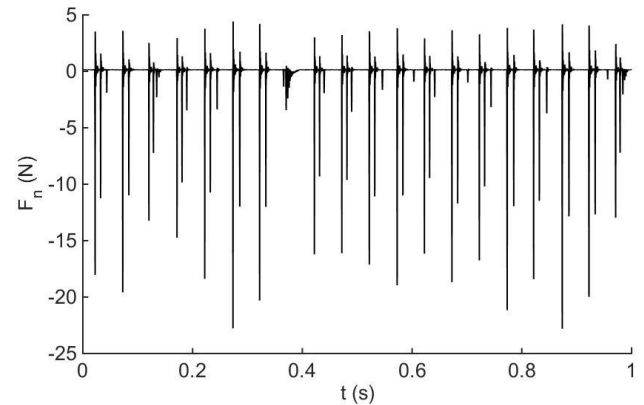


FIGURE 3. LARGE TIME SCALE EVOLUTION OF F_n

Short time scale

Figure 4 shows time evolution of normal load during a single impact. Contact duration is retrieved from the main peak of normal load and usually ranges from 0.4 to 0.8 ms. The main peak of load is followed by several damped oscillations which highlight a dynamic response of the test rig following the impact. This response is supposed to have a minimal influence on the value of the maximal load amplitude as the bell-shaped normal load curve remains mostly undisturbed.

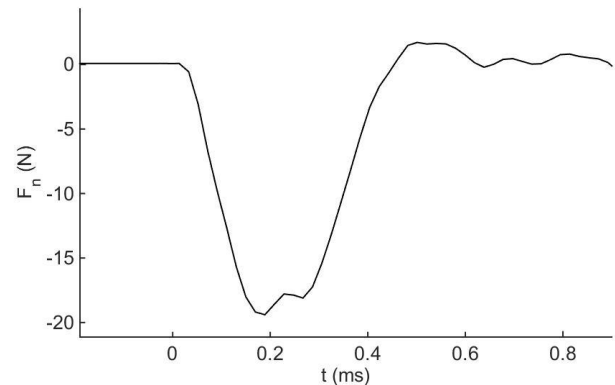


FIGURE 4. SHORT SCALE TIME EVOLUTION OF F_n DURING IMPACT

Wear characteristics

Observed wear scars are typically oval and their shapes give information about the mechanical processes that take place during impacts. Material is either removed as wear debris or displaced by plastic deformation. Thus, positive volumes correspond to displaced material and natural volumes correspond to removed material.

In the following, wear volumes W_{tot} and W_{imp} are defined as natural volume and natural volume per impact, that is to say difference between positive and negative measured volumes. In this way, only removed material is taken into account.

EXPERIMENTAL RESULTS AND DISCUSSION

Impact duration and $\bar{\mu}$

Observed impact durations range from 0.5 to 0.9 ms and the corresponding load curve is systematically bell-shaped.

Figure 5 shows average impact duration \bar{t}_{imp} versus $\bar{\mu}$ defined as the average of instantaneous ratio between F_t and F_n during a complete test. \bar{t}_{imp} increases with $\bar{\mu}$, from 0.5 ms for normal impacts to 0.9 ms for impacts with a high tangential component. This increase of \bar{t}_{imp} may highlight an increase of the sliding distance δ_t during contact.

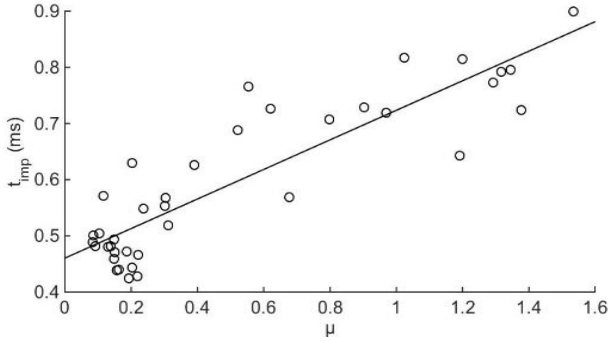


FIGURE 5. IMPACT DURATION VERSUS $\bar{\mu}$

Instantaneous ratio $\bar{\mu}$ and incidence angle

Experiments with various incidence angles are performed and $\bar{\mu}$ is observed to be inversely proportional to incidence angle (Figure 6). The linear dependence between $\bar{\mu}$ and $\bar{\alpha}$ is expressed in equation (2) and is consistent with previous observations [13].

As $\bar{\mu}$ and $\bar{\alpha}$ are interrelated, $\bar{\mu}$ can be considered as a primary parameter for the following wear analyses. $\bar{\alpha}$ is then a test parameter that can be easily set up with the aim of getting a specific value for $\bar{\mu}$ during experiment.

$$\bar{\mu} = -0.02\bar{\alpha} + 1.9 \quad (15^\circ \leq \bar{\alpha} \leq 70^\circ) \quad (1)$$

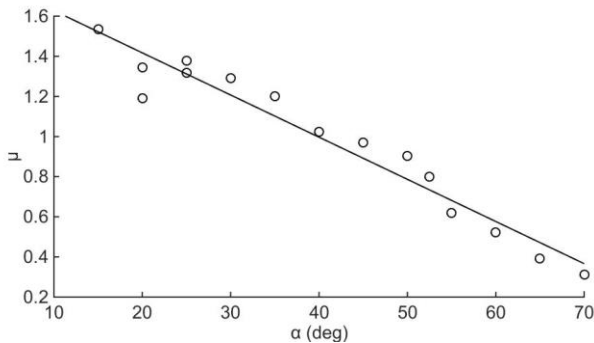


FIGURE 6. $\bar{\mu}$ VERSUS INCIDENCE ANGLE

Incidence angle and wear

Wear volume is still compared with $\bar{\alpha}$ to make the connection with erosive wear models (Figure 7). Indeed, most of these models relate wear with incidence angle [15–19].

Experimental results show that wear increases as the incidence angle is more and more grazing. These experimental values are compared to the erosive wear model of Brach [15,20] and Sundararajan [19] in which a normalized shear energy T^* is introduced (equations (3) and (4)). In this model, wear volume is assumed to be proportional to this shear energy.

$$T^* = \frac{1}{(1+\lambda)\mu_c} \left(2 - \frac{\bar{\mu}}{\mu_c}\right) \cos^2 \bar{\alpha} \quad (2)$$

$$\mu_c = \frac{1}{(1+\lambda)(1+e)\tan \bar{\alpha}} \quad (3)$$

T^* is defined as a dimensionless energy transferred to target during an impact. This definition takes two sources of energy dissipation into account: an energy associated with the impactor rebound (through e) and an energy associated with friction (through $\bar{\mu}$). Considering asperities as spherical erosive particles treated as point masses, it is assumed that $\lambda = 0$. $\bar{\mu}$ is obtained from load measurements during the test. The definition of the restitution coefficient e is chosen as the ratio between rebound velocity and incident velocity. It is measured with a laser vibrometer on several impacts and we obtain in average $e = 0.85$.

In the range $[15^\circ 90^\circ]$, the experimental results match very well with the evolution of Brach normalized shear energy. This result confirms that erosive models can be relevant to describe wear of macroscopic bodies [14].

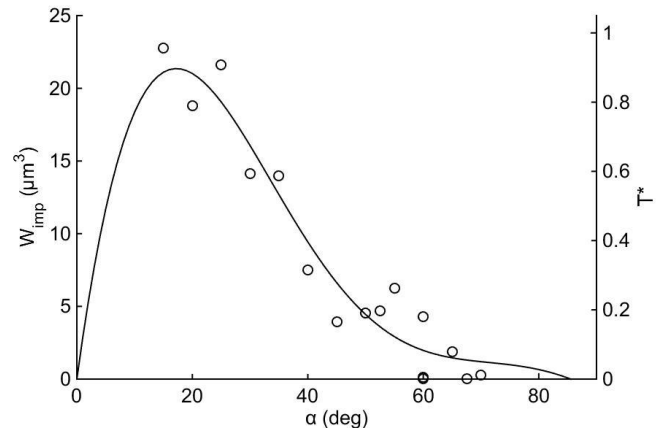


FIGURE 7. EVOLUTION OF T^* (-) AND W_{imp} (o) VERSUS $\bar{\alpha}$

Instantaneous ratio $\bar{\mu}$ and wear

Wear is compared with $\bar{\mu}$ (Figure 8). As $\bar{\mu}$ and $\bar{\alpha}$ are interrelated according to a nearly linear relation (equation (2)), it is consistent to find that wear increases with $\bar{\mu}$. It is interesting to note that $\bar{\mu} = 1$ seems to be a transitional value between two wear modes. Observed wear for $\bar{\mu} > 1$ is much more important than for $\bar{\mu} < 1$.

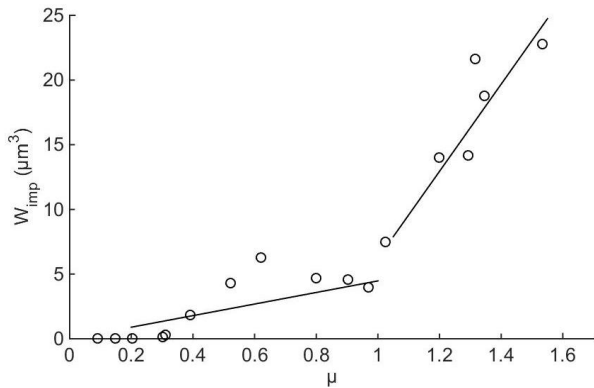


FIGURE 8. W_{imp} VERSUS $\bar{\mu}$

CONCLUSION

Impact wear between two steel cylinders is studied. Experiments are performed and influence of $\bar{\mu}$ on impact duration is highlighted as well the linear dependence between $\bar{\mu}$ and $\bar{\alpha}$. The influence of $\bar{\mu}$ on wear is highlighted and experimental results are compared to an erosive wear model. These results confirm the importance of shear stress on wear formation and show that $\bar{\mu}$ is a primary wear parameter and not $\bar{\alpha}$ as it is often considered in erosive wear models.

Further work is in progress and aims at adapting the test rig in order to make impacts between real heat exchanger tubes and AVB instead of steel cylinders. In this way, experimental contact geometry and materials will be more consistent with the real ones. Displacement of the impactor will also be measured in order to obtain information about incidence and rebound velocities and angles and about sliding distance during impact.

REFERENCES

- [1] Phalippou, C., Herms, E., and Ruffet, F., 2013, "PWR steam generator tube and AVB wear under perpendicular impacting," Proc. ASME 2013 Press. Vessel. Pip. Conf.
- [2] Ko, P., 1987, "Metallic wear—a review with special references to vibration-induced wear in power plant components," Tribol. Int., **20**(2), pp. 66–78.
- [3] Bowden, F. P., and Tabor, D., 1954, The Friction and Lubrication of Solids.
- [4] Rabinowicz, E., 1965, "Friction and Wear of Materials."
- [5] Engel, P. A., 1978, Impact Wear of Materials.
- [6] Engel, P. A., 1978, "Percussive impact wear: A study of repetitively impacting solid components in engineering," Tribol. Int., **11**(June), pp. 169–176.
- [7] Engel, P. a., Lyons, T. H., and Sirico, J. L., 1973, "Impact wear model for steel specimens," Wear, **23**(2), pp. 185–201.
- [8] Levy, G., and Morri, J., 1985, "Impact fretting wear in CO₂-based environments," Wear, **106**(1-3), pp. 97–138.
- [9] Connors, H., 1981, "Flow-induced vibration and wear of steam generator tubes," Nucl. Technol.
- [10] Frick, T. M., 1997, "An empirical wear projection technology with steam generator tube applications and relations to work-rate and wear simulations/tests," ASME Flow-Induced Vib. Noise, **2**, pp. 275–282.
- [11] Hofmann, P., Schettler, T., and Steininger, D., 1992, "PWR steam generator tube fretting and fatigue wear phenomena and correlations,," ASME Flow-Induced Vib. Noise, **1**.
- [12] Lewis, R., 2007, "A modelling technique for predicting compound impact wear," Wear, **262**(11-12), pp. 1516–1521.
- [13] Rigaud, E., and Le Bot, A., 2013, "Influence of incidence angle on wear induced by sliding impacts," Wear, **307**(1-2), pp. 68–74.
- [14] Kaiser, A.-L., Bec, S., Vernot, J.-P., and Langlade, C., 2006, "Wear damage resulting from sliding impact kinematics in pressurized high temperature water: energetical and statistical approaches," J. Phys. D. Appl. Phys., **39**(15), pp. 3193–3199.
- [15] Brach, R. M., 1988, "Impact dynamics with applications to solid particle erosion," Int. J. Impact Eng., **7**(1), pp. 37–53.
- [16] Finnie, I., 1960, "Erosion of surfaces by solid particles," Wear, **3**, pp. 87–103.
- [17] Bitter, J. G. a., 1963, "A study of erosion phenomena," Wear, **6**, pp. 169–190.
- [18] Tilly, G., 1973, "A two stage mechanism of ductile erosion," Wear, **23**(1), pp. 87–96.
- [19] Sundararajan, G., 1991, "A comprehensive model for the solid particle erosion of ductile materials," Wear, **149**, pp. 111–127.

- [20] Brach, R. M., 1993, "Classical planar impact theory and the tip impact of a slender rod," *Int. J. Impact Eng.*, **13**(1), pp. 21–33.